

BADM: Batch ADMM for Deep Learning

Ouya Wang, *Member, IEEE*, Shenglong Zhou, and Geoffrey Ye Li, *Fellow, IEEE*

Abstract—Stochastic gradient descent-based algorithms are widely used for training deep neural networks but often suffer from slow convergence. To address the challenge, we leverage the framework of the alternating direction method of multipliers (ADMM) to develop a novel data-driven algorithm, called batch ADMM (BADM). The fundamental idea of the proposed algorithm is to split the training data into batches, which is further divided into sub-batches where primal and dual variables are updated to generate global parameters through aggregation. We evaluate the performance of BADM across various deep learning tasks, including graph modelling, computer vision, image generation, and natural language processing. Extensive numerical experiments demonstrate that BADM achieves faster convergence and superior testing accuracy compared to other state-of-the-art optimizers.

Index Terms—Deep Learning, Neural Network, Optimization, ADMM, Gradient Descent.



1 INTRODUCTION

DEEP learning (DL) has revolutionized a variety of applications, such as computer vision, natural language processing (NLP), image generation [1], [2], wireless communications [3], [4], to name a few. Central to the success of DL models is the optimization of their parameters, which involves finding the optimal set of weights that minimize a given loss function.

1.1 SGD-based learning algorithms

One of the most popular and effective optimization methods for training deep neural networks (DNNs) is stochastic gradient descent (SGD)-based algorithms. However, these algorithms frequently suffer from slow convergence, especially in high-dimensional and non-convex landscapes [5], resulting in enormous training time. Additionally, they also exhibit high sensitivity to poor conditioning, meaning that even a tiny change in input can significantly alter the gradient [6]. To overcome such a drawback, SGD with momentum (SGDM) [7] has been developed, which introduces the first-order momentum to suppress the oscillation of SGD during training and thus makes the training more robust.

It is noted that SGD or SGDM update parameters using a fixed learning rate. In contrast, the adaptive gradient (AdaGrad) algorithm [8] interpolates second-order momentum, which accumulates second-order gradients to achieve an adaptive learning rate. As the number of updates increases, the second-order momentum enables the accumulation of sufficient knowledge, necessitating a smaller learning rate to avoid excessive influence from individual samples. However, the consistently decreasing learning rate

may prematurely terminate the training process, preventing the acquisition of essential knowledge from subsequent data. Then the root mean squared propagation (RMSProp) [9] has been designed to mitigate the issue by preventing momentum from accumulating all previous gradients. It employs an exponential weighting technique to balance the distant historical information and the knowledge of the current second-order gradients.

As an extensively used tool in DL applications, adaptive moment (Adam) estimation [10] combines the first-order momentum and adaptive learning rates, thereby delivering robustness to hyperparameters. The update rule for individual weights scales their gradients inversely proportional to the ℓ_2 norm of their current and past gradients. When replacing the ℓ_2 norm with an infinite norm, Adamax [10] can be obtained, which generally exhibits more stable behavior. In [11], a Nesterov-accelerated adaptive moment (NAdam) estimation has been developed to enhance Adam by incorporating the tactic of the Nesterov-accelerated gradient method. For more other gradient-based algorithms, we refer to a survey [12] and the references therein.

1.2 ADM and ADMM-based learning algorithms

Given its capability to decompose a large-scale problem into manageable sub-problems, alternating direction methods (ADMs) and alternating direction method of multipliers (ADMM) [13] are appealing tools for addressing challenges in distributed manners, making them promising for DL applications, such as image compressive sensing [14], federated learning [15], reinforcement learning [16], few-shot learning [17], and so forth.

In [18], [19], neural network models have been divided into sets of layers or blocks that satisfy a consistency constraint, ensuring the output of one set of layers matches the input of the next. The constrained model is relaxed by penalizing these constraints, resulting in an unconstrained penalty model that can be solved by ADMs effectively.

Besides ADMs, a separate line of research explored ADMM to process the neural network models. For instance, the neural network model is relaxed in [20] by penalizing all

- O. Wang and G. Li are with the ITP Lab, Department of Electrical and Electronic Engineering, Imperial College London, the United Kingdom (ouya.wang20@imperial.ac.uk, geoffrey.li@imperial.ac.uk).
- S. Zhou is with the School of Mathematics and Statistics, Beijing Jiaotong University, Beijing, China (shlzhou@bjtu.edu.cn).
- This work was supported by the Fundamental Research Funds for the Central Universities and the Talent Fund of Beijing Jiaotong University.
- Corresponding author: S. Zhou.

Manuscript received April 19, 2005; revised August 26, 2015.

equality constraints. Based on the penalty model, a single Lagrange multiplier was added only for the outermost layer, which differs from the standard augmented Lagrange function [13]. Then ADMM is designed to solve the problem. In [21], all equality constraints except, for a linear equation for the outermost layer are penalized. A dlADMM algorithm is then proposed to solve the new penalized model. To avoid the computation of matrix inverses, quadratic approximation is cast to tackle a large-scale system of equations. Similar work can be found in [22]. Fairly recently, an Anderson acceleration is employed in [23] to boost the convergence rate of dlADMM. Moreover, the gradient-free feature of ADMM is leveraged in [24] to develop a sigmoid-ADMM algorithm, which enables mitigating the saturation issue arised from the use of sigmoid activations. This algorithm demonstrates superior performance compared to the conventional SGD methods typically used for ReLU-based networks.

We highlight that all these algorithms have been developed based on the neural network model or its reformulations and thus can be deemed model-driven approaches in certain sense. Numerical experiments have demonstrated that they converge faster and have better generalization performance across various applications than the traditional DL methods. Differing from all prior work, we aim to design a novel data-driven ADMM algorithm in this work.

1.3 Our contribution

The primary contribution of this paper lies in the development of an effective data-driven algorithm, BADM, with several advantageous properties.

- The algorithmic framework is simple but general enough, offering great flexibility to deal with a wide range of applications, including various distributed optimization problems and deep learning models, such as DNNs, Transformers, multilayer perceptron (MLP), convolutional neural networks (CNNs), graph neural networks (GNNs), U-Net, to name a few.
- Distinct from the conventional ADMM paradigms, such as dlADMM [22] and sigmoid-ADMM [24], which are developed based on the neural network models, our proposed algorithm can be deemed as a data-driven method. Specifically, we partition the training data into a series of batches and further subdivide each batch into multiple sub-batches. Based on this data partitioning, we construct an optimization model, as presented in models (3) and (4), to develop BADM. A detailed comparison of BADM with other ADMM algorithms is provided in Section 3.
- The proposed algorithm enables parallel computing for sub-problems using sub-batch data, resulting in low computational complexity. Extensive numerical experiments on applications in graph modelling, computer vision, image generation, and NLP demonstrate the high performance of BADM. To be more precise, it achieves higher testing accuracy in most classification tasks, improves training efficiency for image generation models by 3.2 times, and reduces pre-training computation time for language modelling by up to 4 times.

1.4 Organization

The paper is organized as follows. In Section 2, we introduce the optimization model based on data partitioning and develop the BADM algorithm. Section 3 provides a detailed comparison of BADM with other ADMM algorithms. In Section 4, we present comprehensive numerical experiments across four different types of tasks: graph modelling, computer vision, image generation, and NLP. Concluding remarks are given in the last section.

2 BADM ALGORITHM

In this section, we begin by introducing the notation that will be used throughout the article and then go through the model formulation and algorithmic design.

2.1 Notation

Throughout the paper, scalars are represented using plain letters, vectors are denoted with bold letters, and matrices are indicated with bold capital letters. We define three sets $\mathbb{B} := \{1, 2, \dots, B\}$, $\mathbb{N} := \{1, 2, \dots, N\}$, $\mathbb{N}_b := \{1, 2, \dots, N_b\}$, and denote $\mathbb{M} := \mathbb{B} \times \mathbb{N}_b$. We use b and n to indicate their elements, namely $b \in \mathbb{B}$, $n \in \mathbb{N}_b$, and $(b, n) \in \mathbb{M}$. Here $:=$ means define. The cardinality of a set \mathcal{D} is written as $|\mathcal{D}|$. For two vectors \mathbf{w} and $\boldsymbol{\pi}$, their inner product is denoted by $\langle \mathbf{w}, \boldsymbol{\pi} \rangle := \sum_i w_i \pi_i$. Let $\|\cdot\|$ be the Euclidean norm, namely, $\|\mathbf{w}\|^2 = \langle \mathbf{w}, \mathbf{w} \rangle$. In the sequel, subscripts i , b , and n respectively represent the index of a sample, a batch, and a sub-batch (e.g., \mathbf{x}_i , \mathcal{D}_b , and \mathcal{D}_{bn}). We use superscript ℓ to stand for the iteration number (e.g., \mathbf{w}_b^ℓ and \mathbf{w}_{bn}^ℓ).

2.2 Model Description

Suppose we are given a set of data as $\mathcal{D} := \{(\mathbf{x}_i, \mathbf{y}_i) : i = 1, 2, \dots, N\}$, where \mathbf{x}_i and \mathbf{y}_i are the input and output/label of the i -th sample, and N is the total number of samples. Recall that $\mathbb{N} := \{1, 2, \dots, N\}$ consists of the indices of all samples. The loss function on this set of data is defined by,

$$F(\mathbf{w}; \mathcal{D}) := \frac{1}{N} \sum_{i \in \mathbb{N}} l(f(\mathbf{w}; \mathbf{x}_i), \mathbf{y}_i), \quad (1)$$

where $l(\cdot)$ is a loss function, $f(\mathbf{w}; \mathcal{D})$ is a function (such as linear functions or neural networks) parameterized by \mathbf{w} and sampled by \mathcal{D} . As presented in Figure 1, we first divide total data indices \mathbb{N} into B disjoint batches, namely, $\mathbb{N} = \mathbb{N}_1 \cup \mathbb{N}_2 \cup \dots \cup \mathbb{N}_B$ and $\mathbb{N}_b \cap \mathbb{N}_{b'} = \emptyset$ for any two distinct b and b' . Differing from the standard settings designed for the SGD algorithms, in the sequel, we introduce a distributed learning scheme. To proceed with that, as shown in Figure 1, we further separate batch \mathbb{N}_b into N_b disjoint sub-batches, that is, $\mathbb{N}_b = \mathbb{N}_{b1} \cup \mathbb{N}_{b2} \cup \dots \cup \mathbb{N}_{bN_b}$ and $\mathbb{N}_{bn} \cap \mathbb{N}_{bn'} = \emptyset$ for any two distinct n and n' . By denoting

$$\begin{aligned} \alpha_{bn} &:= \frac{|\mathbb{N}_{bn}|}{|\mathbb{N}|} = \frac{|\mathbb{N}_{bn}|}{N}, \\ \alpha_b &:= \sum_{n \in \mathbb{N}_b} \alpha_{bn}, \\ F_{bn}(\mathbf{w}) &:= \frac{1}{|\mathbb{N}_{bn}|} \sum_{i \in \mathbb{N}_{bn}} l(f(\mathbf{w}; \mathbf{x}_i), \mathbf{y}_i), \end{aligned} \quad (2)$$

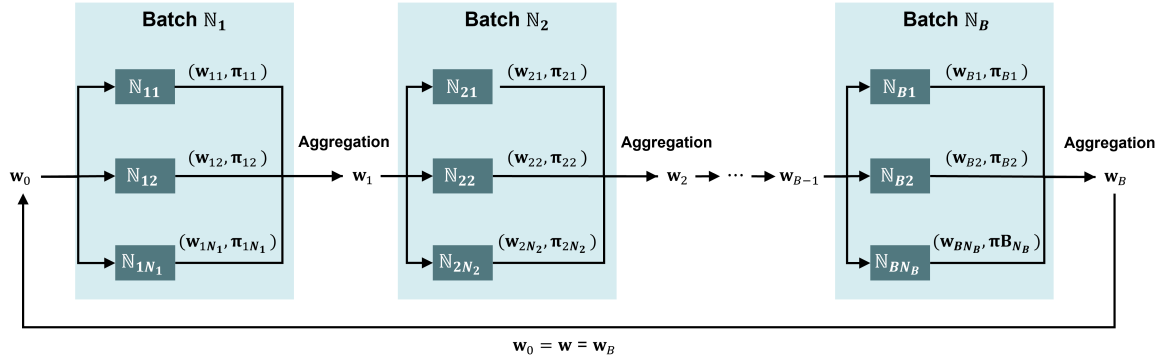


Fig. 1: Data split and each iteration of BADM.

we can rewrite $F(\mathbf{w}; \mathcal{D})$ as follows,

$$\begin{aligned} F(\mathbf{w}; \mathcal{D}) &= \frac{1}{N} \sum_{b \in \mathbb{B}} \sum_{n \in \mathbb{N}_b} \sum_{i \in \mathbb{N}_{bn}} l(f(\mathbf{w}; \mathbf{x}_i), \mathbf{y}_i) \\ &= \sum_{b \in \mathbb{B}} \sum_{n \in \mathbb{N}_b} \alpha_{bn} F_{bn}(\mathbf{w}). \end{aligned}$$

Note that $\sum_{b \in \mathbb{B}} \sum_{n \in \mathbb{N}_b} \alpha_{bn} = 1$. Overall, the goal is to learn an optimal parameter \mathbf{w}^* by

$$\mathbf{w}^* = \arg \min_{\mathbf{w}} F(\mathbf{w}; \mathcal{D}) = \arg \min_{\mathbf{w}} \sum_{b \in \mathbb{B}} \sum_{n \in \mathbb{N}_b} \alpha_{bn} F_{bn}(\mathbf{w}). \quad (3)$$

2.3 Algorithmic Design

In order to adopt the ADMM algorithm, we rewrite problem (3) as follows,

$$\begin{aligned} \min_{\mathbf{w}, \mathbf{w}_{bn}} \quad & \sum_{b \in \mathbb{B}} \sum_{n \in \mathbb{N}_b} \alpha_{bn} F_{bn}(\mathbf{w}_{bn}), \\ \text{s.t.} \quad & \mathbf{w} = \mathbf{w}_{bn}, \quad b \in \mathbb{B}, \quad n \in \mathbb{N}_b. \end{aligned}$$

Besides the global parameter \mathbf{w} , additional variables \mathbf{w}_{bn} (i.e., the local parameter for sub-batch \mathcal{D}_{bn}) are introduced in the above model. The corresponding augmented Lagrange function is,

$$\begin{aligned} \mathcal{L}(\mathbf{w}, \{(\mathbf{w}_{bn}, \boldsymbol{\pi}_{bn}) : (b, n) \in \mathbb{M}\}) \\ := \sum_{b \in \mathbb{B}} \sum_{n \in \mathbb{N}_b} \alpha_{bn} \mathcal{L}_{bn}(\mathbf{w}, \boldsymbol{\pi}_{bn}, \mathbf{w}_{bn}), \end{aligned}$$

where \mathcal{L}_{bn} is given by

$$\begin{aligned} \mathcal{L}_{bn}(\mathbf{w}, \mathbf{w}_{bn}, \boldsymbol{\pi}_{bn}) \\ := F_{bn}(\mathbf{w}_{bn}) + \langle \boldsymbol{\pi}_{bn}, \mathbf{w}_{bn} - \mathbf{w} \rangle + \frac{\sigma}{2} \|\mathbf{w}_{bn} - \mathbf{w}\|^2. \end{aligned}$$

and $\sigma > 0$. Here $\{\boldsymbol{\pi}_{bn} : (b, n) \in \mathbb{M}\}$ are the Lagrange multipliers. The framework of ADMM is given as follows. By giving $(\mathbf{w}^0, \{(\mathbf{w}_{bn}^0, \boldsymbol{\pi}_{bn}^0) : (b, n) \in \mathbb{M}\})$, we perform the following steps iteratively for each iteration $\ell \in \{0, 1, 2, \dots\}$ and each $b \in \mathbb{B}$,

$$\mathbf{w}_{bn}^{\ell+1} = \arg \min_{\mathbf{w}_{bn}} \mathcal{L}_{bn}(\mathbf{w}_{bn}^{\ell+1}, \mathbf{w}_{bn}, \boldsymbol{\pi}_{bn}^{\ell}), \quad n \in \mathbb{N}_b, \quad (4a)$$

$$\boldsymbol{\pi}_{bn}^{\ell+1} = \boldsymbol{\pi}_{bn}^{\ell} + \sigma(\mathbf{w}_{bn}^{\ell+1} - \mathbf{w}_{bn}^{\ell+1}), \quad n \in \mathbb{N}_b, \quad (4b)$$

$$\mathbf{w}_b^{\ell+1} = \arg \min_{\mathbf{w}} \sum_{n \in \mathbb{N}_b} \alpha_{bn} \mathcal{L}_{bn}(\mathbf{w}, \mathbf{w}_{bn}^{\ell+1}, \boldsymbol{\pi}_{bn}^{\ell+1}), \quad (4c)$$

where $\mathbf{w}_0^{\ell+1} = \mathbf{w}^{\ell} = \mathbf{w}_B^{\ell}$. To accelerate the computational speed, we solve sub-problems for \mathbf{w}_{bn} inexactly by

$$\begin{aligned} \mathbf{w}_{bn}^{\ell+1} &= \arg \min_{\mathbf{w}_{bn}} \langle \boldsymbol{\pi}_{bn}^{\ell}, \mathbf{w}_{bn} \rangle + \frac{\sigma}{2} \|\mathbf{w}_{bn} - \mathbf{w}_{bn}^{\ell+1}\|^2 \\ &\quad + \langle F'_{bn}(\mathbf{w}_{bn}^{\ell+1}), \mathbf{w}_{bn} \rangle + \frac{\rho}{2} \|\mathbf{w}_{bn} - \mathbf{w}_{bn}^{\ell+1}\|^2 \\ &= \mathbf{w}_{bn}^{\ell+1} - \frac{F'_{bn}(\mathbf{w}_{bn}^{\ell+1}) + \boldsymbol{\pi}_{bn}^{\ell}}{\rho + \sigma}, \end{aligned} \quad (5)$$

where $\rho > 0$ and $F'_{bn}(\mathbf{w})$ is one of elements in the sub-differential (denoted by $\partial F_{bn}(\mathbf{w})$, see [25, Definition 8.3], of $F_{bn}(\mathbf{w})$. Note that $F'_{bn}(\mathbf{w})$ is the gradient of $F_{bn}(\mathbf{w})$ if it is continuously differentiable at \mathbf{w} .

The sub-problems with respect to \mathbf{w}_b can be solve by

$$\begin{aligned} \mathbf{w}_b^{\ell+1} &= \arg \min_{\mathbf{w}} \sum_{n \in \mathbb{N}_b} \alpha_{bn} \left(\frac{\sigma}{2} \|\mathbf{w}_{bn}^{\ell+1} - \mathbf{w}\|^2 - \langle \boldsymbol{\pi}_{bn}^{\ell+1}, \mathbf{w} \rangle \right) \\ &= \sum_{n \in \mathbb{N}_b} \frac{\alpha_{bn}}{\alpha_b} \left(\mathbf{w}_{bn}^{\ell+1} + \frac{\boldsymbol{\pi}_{bn}^{\ell+1}}{\sigma} \right). \end{aligned}$$

To improve the learning performance, we incorporate the second moment to determine an adaptive learning rate when updating $\mathbf{w}_b^{\ell+1}$. This approach has demonstrated effectiveness in popular optimizers, such as Adam and RMSprop. To be specific, given \mathbf{m}_{bn}^0 and $\beta \in (0, 1)$, let

$$\mathbf{m}_{bn}^{\ell+1} = \beta \mathbf{m}_{bn}^{\ell} + (1 - \beta) \boldsymbol{\pi}_{bn}^{\ell+1} \odot \boldsymbol{\pi}_{bn}^{\ell+1}, \quad (6)$$

Then update $\mathbf{w}_b^{\ell+1}$ by

$$\mathbf{w}_b^{\ell+1} = \sum_{n \in \mathbb{N}_b} \frac{\alpha_{bn}}{\alpha_b} \left(\mathbf{w}_{bn}^{\ell+1} + (\mathbf{m}_{bn}^{\ell+1})^{-\frac{1}{2}} \odot \frac{\boldsymbol{\pi}_{bn}^{\ell+1}}{\sigma} \right), \quad (7)$$

where symbol \odot stands for the Hadamard product and $\mathbf{m}^{-1/2}$ is a vector with the i -th entry being $1/\sqrt{m_i}$. It is noted that by initializing $\mathbf{m}_{bn}^0 > \mathbf{0}$ we have $\mathbf{m}_{bn}^1 \geq \beta \mathbf{m}_{bn}^0 > \mathbf{0}$ from (6). Therefore, by the induction, we can claim that $\mathbf{m}_{bn}^{\ell} > \mathbf{0}$ for any ℓ , which indicates $(\mathbf{m}_{bn}^{\ell+1})^{-1/2}$ always exists and thus (7) is well defined. The overall algorithmic framework is presented in Algorithm 1, also referred to Figure 1. Its advantageous properties are highlighted as follows.

- **Comparable computational complexity.** The primary computational expense in Algorithm 1 arises from computing $F'_{bn}(\mathbf{w}^{\ell})$ for each sub-batch \mathbb{N}_{bn} . Consequently, its computational burden resembles that of standard

Algorithm 1: Batch ADMM (BADM)

Divide data \mathcal{D} into B disjoint batches $\{\mathbb{N}_1, \mathbb{N}_2, \dots, \mathbb{N}_B\}$ and split batch data \mathbb{N}_b into N_b disjoint sub-batches $\{\mathbb{N}_{b1}, \mathbb{N}_{b2}, \dots, \mathbb{N}_{bN_b}\}$ for each $b \in \mathbb{B}$. Calculate α_{bn} and α_b by (2) for each $(b, n) \in \mathbb{M}$. Initialize $(\sigma, \rho, L) > 0$, $\beta \in (0, 1)$, and $(\mathbf{w}^0, \{(\mathbf{w}_{bn}^0, \boldsymbol{\pi}_{bn}^0, \mathbf{m}_{bn}^0) : (b, n) \in \mathbb{M}\})$.

for $\ell = 0, 1, 2, \dots, L$ **do**

Initial $\mathbf{w}_0^{\ell+1} = \mathbf{w}^\ell$ for batch \mathbb{N}_1 .

for $b = 1, 2, \dots, B$ **do**

for $n = 1, 2, \dots, N_b$ **do**

Update $(\mathbf{w}_{bn}^{\ell+1}, \boldsymbol{\pi}_{bn}^{\ell+1}, \mathbf{m}_{bn}^{\ell+1})$ by (5), (4b) and (6), respectively.

end

Update $\mathbf{w}_b^{\ell+1}$ by (7).

end

Update global parameter $\mathbf{w}^{\ell+1} = \mathbf{w}_B^{\ell+1}$.

end

Return \mathbf{w}^ℓ .

SGD-based algorithms. Hence, Algorithm 1 does not exhibit higher computational complexity compared to most widely-used algorithms.

- **Parallel computing.** Within each batch b , N_b blocks of parameters $(\mathbf{w}_{b1}^\ell, \boldsymbol{\pi}_{b1}^\ell, \mathbf{m}_{b1}^\ell), \dots, (\mathbf{w}_{bN_b}^\ell, \boldsymbol{\pi}_{bN_b}^\ell, \mathbf{m}_{bN_b}^\ell)$ can be computed in parallel, enabling fast computation.

3 ALGORITHM COMPARISON

The conventional neural network model takes the form of

$$\begin{aligned} \min_{\mathbf{W}, \mathbf{V}} L(\mathbf{V}_N, \mathbf{Y}), \\ \text{s.t. } \mathbf{V}_i = \varphi_i(\mathbf{W}_i \mathbf{V}_{i-1}), i = 1, 2, \dots, N, \end{aligned} \quad (8)$$

where L is the loss function, e.g., the average mean squared error [24], φ_i is the activation function for the i -th layer (e.g., ReLU or sigmoid for inner layers and softmax or linear functions for the outermost layer), $\mathbf{W} := (\mathbf{W}_1, \mathbf{W}_2, \dots, \mathbf{W}_N)$, $\mathbf{V} = (\mathbf{V}_0, \mathbf{V}_1, \dots, \mathbf{V}_N)$, $\mathbf{Y} := (\mathbf{y}_1, \mathbf{y}_2, \dots, \mathbf{y}_N)$, and $\mathbf{V}_0 := (\mathbf{x}_1, \mathbf{x}_2, \dots, \mathbf{x}_N)$. Let $\|\cdot\|_F$ be the Frobenius norm. Then the augmented Lagrange function of the above problem is

$$\begin{aligned} \mathcal{L}(\mathbf{W}, \mathbf{V}, \boldsymbol{\Lambda}) = L(\mathbf{V}_N, \mathbf{Y}) + \sum_{i=1}^N (\langle \mathbf{V}_i - \varphi_i(\mathbf{W}_i \mathbf{V}_{i-1}), \boldsymbol{\Lambda}_i \rangle \\ + \frac{\sigma}{2} \|\mathbf{V}_i - \varphi_i(\mathbf{W}_i \mathbf{V}_{i-1})\|_F^2). \end{aligned}$$

The scheme of ADMM usually updates \mathbf{W}_i in the backward order as $\mathbf{W}_N \rightarrow \dots \rightarrow \mathbf{W}_2 \rightarrow \mathbf{W}_1$, then updates \mathbf{V}_i in the forward order as $\mathbf{V}_1 \rightarrow \mathbf{V}_2 \dots \rightarrow \mathbf{V}_N$, and finally updates multipliers $\boldsymbol{\Lambda}_i$ in parallel. To be more specific, at iteration ℓ , \mathbf{W}_i , \mathbf{V}_i , and $\boldsymbol{\Lambda}_i$ are updated by

$$\begin{aligned} \mathbf{W}_i^{\ell+1} &= \operatorname{argmin}_{\mathbf{W}_i} \langle \mathbf{V}_i^\ell - \varphi_i(\mathbf{W}_i \mathbf{V}_{i-1}^\ell), \boldsymbol{\Lambda}_i^\ell \rangle \\ &\quad + \frac{\sigma}{2} \|\mathbf{V}_i^\ell - \varphi_i(\mathbf{W}_i \mathbf{V}_{i-1}^\ell)\|_F^2, i = N, N-1, \dots, 1, \\ \mathbf{V}_i^{\ell+1} &= \operatorname{argmin}_{\mathbf{V}_i} \langle \mathbf{V}_i - \varphi_i(\mathbf{W}_i^{\ell+1} \mathbf{V}_{i-1}^{\ell+1}), \boldsymbol{\Lambda}_i^\ell \rangle \\ &\quad + \frac{\sigma}{2} \|\mathbf{V}_i - \varphi_i(\mathbf{W}_i^{\ell+1} \mathbf{V}_{i-1}^{\ell+1})\|_F^2, i = 1, 2, \dots, N, \\ \mathbf{V}_N^{\ell+1} &= \operatorname{argmin}_{\mathbf{V}_N} l(\mathbf{V}_N, \mathbf{Y}) + \langle \mathbf{V}_N - \varphi_i(\mathbf{W}_N^{\ell+1} \mathbf{V}_{N-1}^{\ell+1}), \boldsymbol{\Lambda}_N^\ell \rangle \\ &\quad + \frac{\sigma}{2} \|\mathbf{V}_N - \varphi_i(\mathbf{W}_N^{\ell+1} \mathbf{V}_{N-1}^{\ell+1})\|_F^2, \\ \boldsymbol{\Lambda}_i^{\ell+1} &= \boldsymbol{\Lambda}_i^\ell + \sigma(\mathbf{V}_i^{\ell+1} - \varphi_i(\mathbf{W}_i^{\ell+1} \mathbf{V}_{i-1}^{\ell+1})), i = 1, 2, \dots, N. \end{aligned}$$

where $\mathbf{V}_0^\ell = \mathbf{V}_0$ for all ℓ . We note that both dlADMM [22] and sigmoid-ADMM [24] follow similar structures of the above algorithm. However, our proposed algorithm is fundamentally different from them. Firstly, the above ADMM framework is based directly on DNN model (8) or its variants, such as the penalty model in [22]. In contrast, BADM is developed based on model (4), which is driven by data partitioning. Furthermore, in BADM, all \mathbf{w}_{bn} , \mathbf{w}_b , and \mathbf{w} can be deemed as \mathbf{W} in model (8). Consequently, dlADMM and sigmoid-ADMM update each portion \mathbf{W}_i of \mathbf{W} sequentially in each iteration, whereas BADM treats \mathbf{w} as a whole entity and updates it all at once in each iteration.

4 EVALUATION OF BADM

This section evaluates the performance of BADM and compare it with several leading optimizers across four different tasks: graph modelling, computer vision, image generation, and NLP. Specifically, for graph modelling, we compare BADM against six benchmarks: Adam, RMSProp, AdaGrad, SGD, NAdam, and dlADMM. For the other three tasks, we compare BADM with Adam and RMSProp. All optimizers use their default hyperparameters as provided by TensorFlow's built-in functions, without any regularization or decay functions applied during training.

4.1 Graph Modelling

We undertake two tasks in graph modelling. The first task is node-level classification, which predicts node categories based on node features and their relationships with other nodes. To evaluate this task, we take advantage of two deep learning structures: DNN and GNN. The second task is graph-level prediction, where we use a message passing neural network (MPNN) to predict the molecular property known as blood-brain barrier permeability (BBBP).

a) Node classification. Following the methodology outlined in [26], we use identical network structures for both DNN and GNN and only modify the training process. Our evaluation encompasses six benchmark datasets: 'Cora', 'Pubmed', 'Citeseer' [27], 'Coauthor CS', 'Coauthor Physics' [28], and 'AMZ Computers'. The first five datasets are extracted from citation networks, where nodes represent publications and edges denote citations. The last dataset, 'AMZ Computers', comprises a co-purchase graph from Amazon, where nodes represent products, edges indicate co-purchase relations, and features are bag-of-words vectors from product reviews. For DNN experiments, we use only node features for classification, whereas in the GNN experiments, we include relations between publications and products as edge features. The data statistics are similar for all datasets. For example, 'Cora' contains 2,708 scientific papers, each classified into one of seven categories. The citation network includes 5,429 links between these papers. Each paper is represented by a binary word vector of length 1,433, indicating the presence of specific words, resulting in 1,433-dimensional node features. The edge features indicate whether two papers cite each other.

We employ a DNN with two hidden layers and 32 neurons in each layer for these experiments. The GNN model follows the structure in [26]. It begins by preprocessing

TABLE 1: Hyperparameters and testing accuracy for node classification.

	Cora	Citeseer	PubMed	Physics	CS	Computers
B	128	512	512	512	512	512
N_b	16	64	128	128	256	128
ρ	200	600	300	500	950	400
σ	800	400	700	500	50	600
DNN						
SGD	0.3034	0.2263	0.3852	0.6937	0.2645	0.3708
AdaGrad	0.7215	0.7243	0.8411	0.9597	0.8593	0.6859
dIADMM	0.3428	0.4084	0.5897	0.8138	0.5716	0.5538
RMSProp	0.7200	0.7334	0.8712	0.9683	0.9176	0.8316
Adam	0.7358	0.7263	0.8731	0.9689	0.9094	0.8243
NAdam	0.7343	0.7323	0.8727	0.9688	0.9176	0.8216
BADM	0.7464	0.7424	0.8736	0.9695	0.9185	0.8403
GNN						
SGD	0.6302	0.1982	0.3676	0.6937	0.3007	0.3711
AdaGrad	0.7268	0.6771	0.8411	0.9610	0.8523	0.6859
RMSProp	0.7781	0.6881	0.8871	0.9699	0.9412	0.8492
Adam	0.7842	0.6962	0.8873	0.9686	0.9438	0.8463
NAdam	0.7857	0.6911	0.8864	0.9687	0.9438	0.8476
BADM	0.7925	0.7213	0.8922	0.9688	0.9495	0.8400

node features using a DNN (with the same structure as in the previous experiment) to create initial representations. Then, two graph convolutional layers with skip connections are applied to generate node embeddings. Post-processing with a DNN refines these embeddings, which are then passed through a Softmax layer to predict node classes. The learning rate is set to 0.001 for all optimizers, while for BADM we maintain (ρ, σ) to satisfy $1/(\rho + \sigma) = 0.001$, such as $(\rho, \sigma) = (200, 800)$ for dataset ‘Cora’. Specific hyperparameters for the six datasets are given in Table 1.

As reported in Table 1, BADM attains the highest testing accuracy for most cases among all optimizers. Moreover, from Fig. 2, BADM has the fastest convergence speed. Although the GNN trained by BADM does not achieve the best testing accuracy when classifying dataset ‘Computers’ (resp. ‘Physics’), BADM only requires 2,300 (resp. 700) training iterations to reach that accuracy, while the others need at least 6,800 (resp. 1,380) iterations to achieve the same accuracy.

One can observe that Adam and RmsProp, one of the most commonly used tools in DL, perform better than or equal to AdaGrad, SGD, NAdam, and dIADMM. Therefore, we will only select them as benchmarks for the remaining tasks in the sequel.

b) Graph properties prediction. Molecular structures can be naturally represented as an undirected graph and GNNs (e.g., MPNN) have proven effective for predicting molecular properties. The dataset used for this experiment consists of 2,050 molecules, each identified by a name, label, and SMILES string. The blood-brain barrier (BBB) is a membrane that separates the blood from the brain’s extracellular fluid, preventing most drugs from entering

the brain. Studying this barrier is essential for developing new drugs targeting the central nervous system. The dataset labels are binary (1 or 0), indicating whether the molecules can permeate the BBB.

Following the approach introduced by [29], we implement MPNN with three stages: message passing, readout, and classification. In the first stage, the edge network passes messages from the 1-hop neighbours of a node to another using their edge features, which updates the node features. Then a recurrent neural network updates the most recent node state using previous node states, allowing information to transfer from one node to another. The second stage (i.e., the readout) converts the k -step-aggregated node states into graph-level embeddings for each molecule. The last stage employs a two-layer classification network to predict BBBP. Fig. 3b shows that BADM reaches the same testing accuracy as that generated by Adam, which is better than RMSProp. Training accuracy is illustrated in Fig. 3a instead of the loss as the latter fluctuates significantly.

4.2 Computer vision

This section focuses on Computer vision tasks, such as image classification and detection. For the classification task, we implement a CNN with various images with sizes ranging from 32×32 to 256×256 and classes ranging from 3 to 15. For the detection task, we implement a vision transformer (ViT) [30] to train the Caltech 101 dataset to detect an airplane in the given image.

c) Image classification. Six datasets used for this experiment are ‘Cifar-10’, ‘Svhn’, ‘Deep weeds’, ‘Cmaterdb’, ‘Patch Camelyon’, and ‘TF Flowers’. ‘Cifar-10’ includes 60,000 color images of size $32 \times 32 \times 3$, divided into 10 classes with 6,000 images per class. It provides 50,000 images for training and 10,000 images for testing. ‘Svhn’ is designed for digit recognition and contains over 600,000 real-world images, each sized $32 \times 32 \times 3$ and categorized into 10 classes. ‘Deep weeds’ has 17,509 images of size $256 \times 256 \times 3$, capturing 8 different weed species native to Australia along with neighbouring flora. ‘Cmaterdb’ includes handwritten numerals in Bangla, Devanagari, and Telugu, each $32 \times 32 \times 3$ RGB-colored and divided into ten classes. ‘Patch Camelyon’ comprises 327,680 color images of size $96 \times 96 \times 3$ extracted from histopathologic scans of lymph node sections, with each image annotated with a binary label indicating the presence of metastatic tissue. ‘TF Flowers’ contains images of daisies, dandelions, roses, sunflowers, and tulips, each sized $180 \times 180 \times 3$.

The architecture of the CNN consists of several 2D convolutional layers for feature extraction, each with 3×3 kernel size, ReLU activation function, and max-pooling following each output. A fully connected layer with 64 neurons is employed before the final classification layer. The structure of convolutional layers and hyperparameters of experiments are reported in the top of Table 2. The loss progression across iterations for each algorithm training on all datasets is shown in Fig. 4¹. Once again, BADM always attains the lowest training loss at each iteration. Testing

1. Due to significant fluctuation of the training loss curves, we implement moving average with a window size of 10 to smooth out data for these figures.

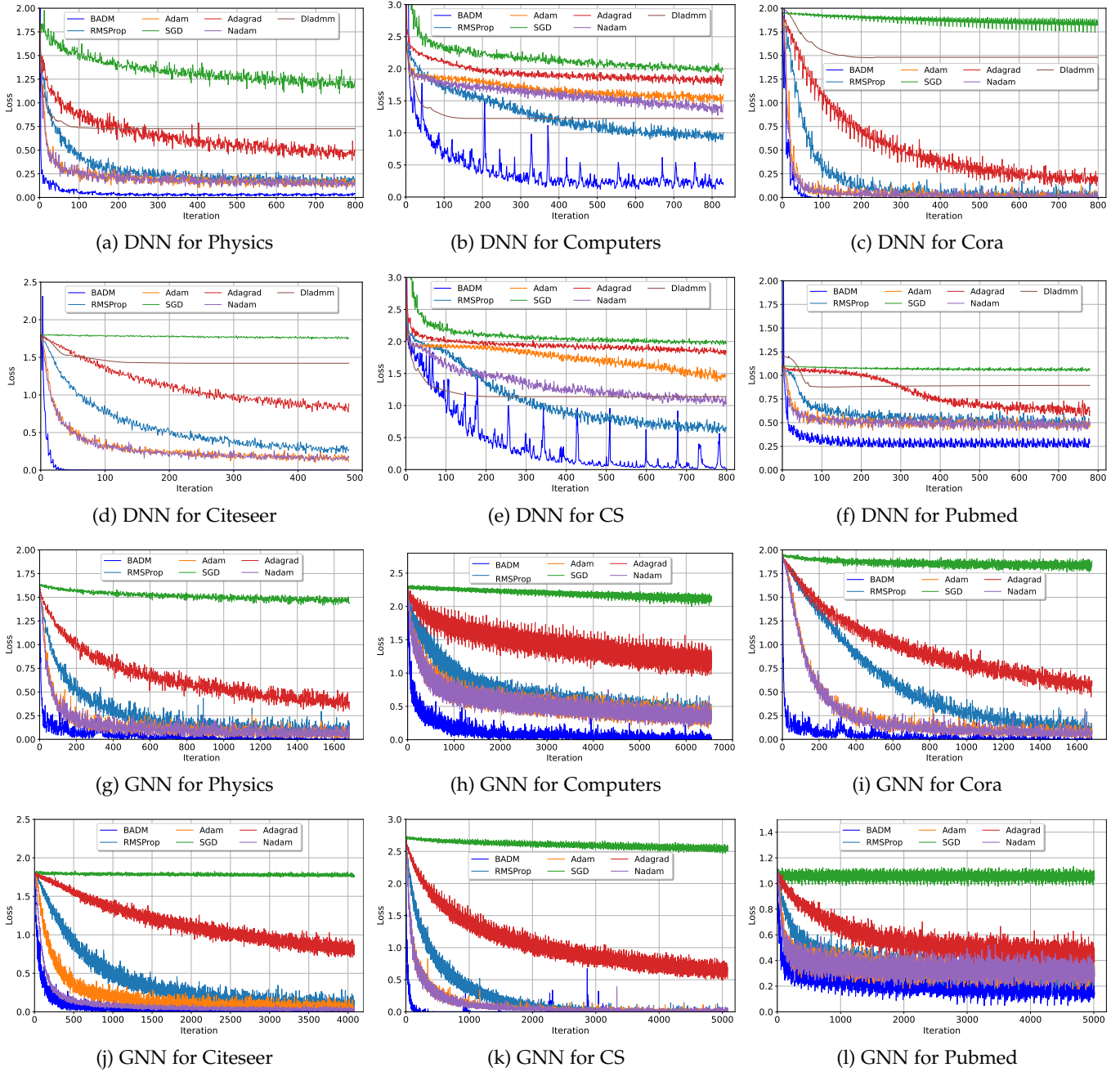


Fig. 2: Training loss v.s. iterations for node classification.

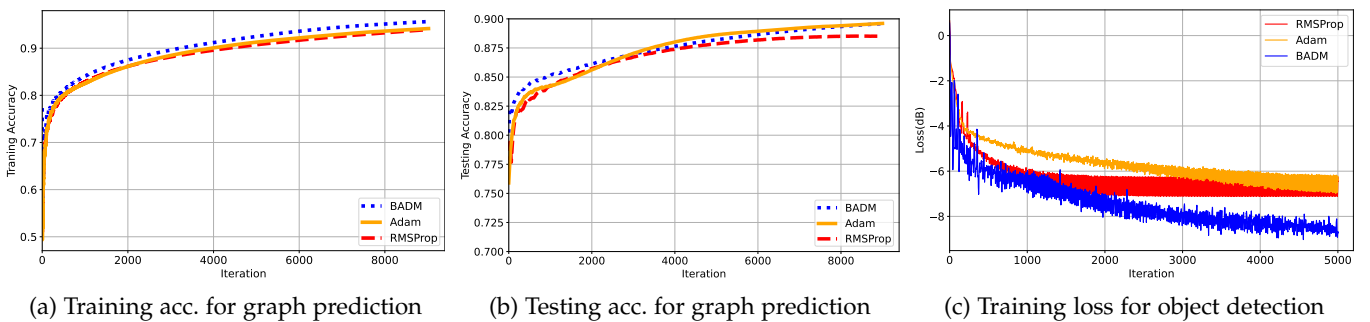


Fig. 3: Performance of three optimizers.

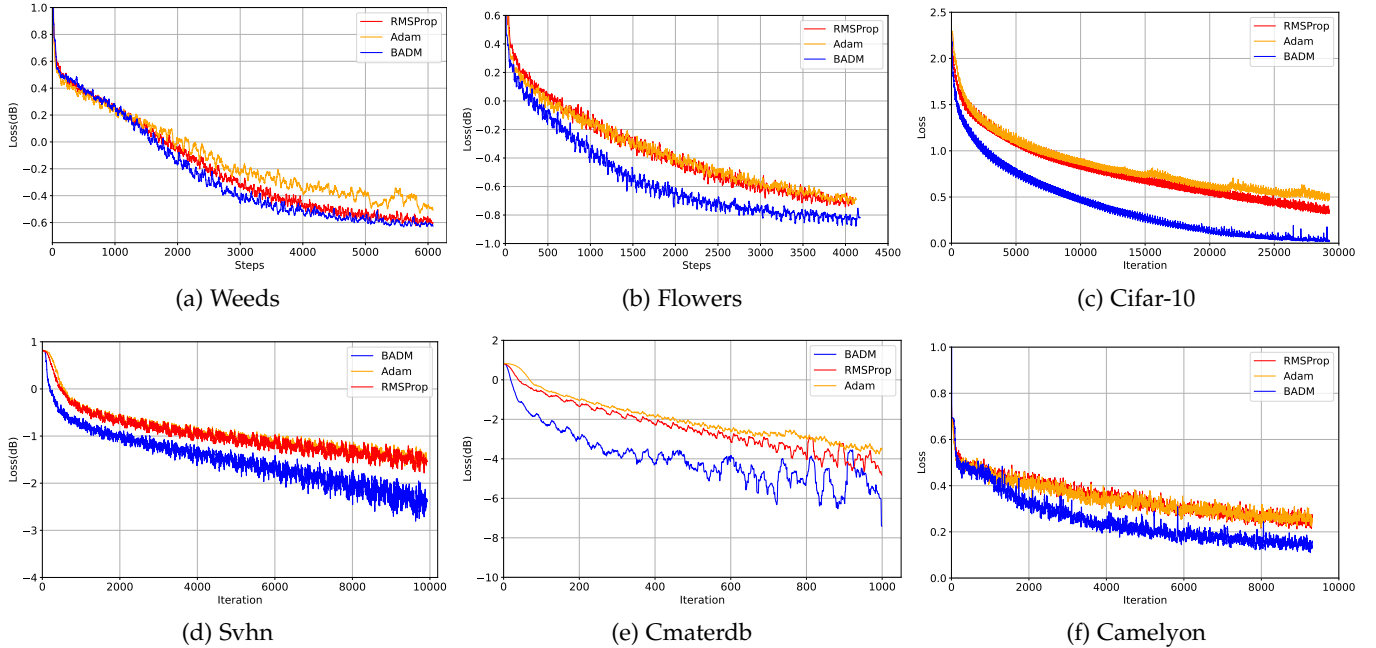


Fig. 4: Training loss v.s. iterations for image classifications.

TABLE 2: Hyperparameters and testing accuracy for image classification.

	Cifar-10	Svhn	Weeds	Cmaterdb	Camelyon	Flowers
B	256	128	64	128	128	64
N_b	64	32	16	32	32	16
ρ	8500	7000	8000	5000	7000	7000
σ	1500	3000	2000	5000	3000	3000
RMSProp	0.7133	0.8946	0.6069	0.9739	0.8425	0.8437
Adam	0.7043	0.8932	0.6171	0.9740	0.8216	0.8593
BADM	0.7149	0.9043	0.6663	0.9750	0.8739	0.9218

accuracy is showcased in rest parts of Table 2. Compared to Adam and RMSProp, BADM attains the highest accuracy for all tasks. One can observe that the accuracy exhibits significant improvement for several challenging datasets, with enhancements of 4.92% and 6.25% observed for ‘Weeds’ and ‘Flowers’, respectively.

d) Object detection. As demonstrated in [30], a ViT has been employed for object detection by predicting bounded box coordinates. Similarly, we train the ViT on the Caltech 101 dataset to detect an airplane in the image. Intersection over union (IOU) serves as a metric to assess the overlap between predicted and true bounded boxes. All optimizers are trained on 640 images with size 224×224 . Fig. 3c² demonstrates that BADM has a faster and more stable convergence along with the training steps increasing. The average testing IOU for BADM, Adam, and RMSProp is 0.9214, 0.9120, and 0.9116, respectively.

2. Moving average with a window size of 10 for this figure.

4.3 Image Generation

Generative models have gained significant attention due to their proficiency in synthesizing realistic images and have shown remarkable success in image generation lately [2], [1]. In this task, we examine the performance of BADM in both conditional and unconditional image synthesis. The evaluation metric is the kernel inception distance (KID), which computes the difference between generated and training distributions within the representation space of a pre-trained InceptionV3 network on ImageNet. A smaller KID value indicates higher similarity, reflecting the superior performance of the algorithm. KID is suitable for small-scale datasets because its expected value is independent of the number of samples it is measured on.

e) Conditional generative adversarial networks (GANs). Compared with conventional GANs, conditional GANs allow us to control the appearance (e.g. class) of the generated samples. In an unconditional GAN, we begin by sampling noise of a fixed dimension from a normal distribution. Moreover, we incorporate class labels to the input channels for both generator (noise input) and discriminator (generated image input). In our experiments, We employ the conditional GAN framework introduced by [31] to perform 32×32 image generation on MNIST and Fashion-MNIST datasets, conditioned on digit classes. The discriminator is a CNN with 2 convolutional layers and one fully connected layer to classify whether the input image is generated or real. The generator consists of one fully connected layer following three convolutional layers to generate images. We employ two datasets, ‘MNIST’ and ‘fashion-MNIST’, to train the conditional GAN. ‘MNIST’ is a dataset containing 70,000 grayscale images of handwritten digits, each sized 28×28 pixels, categorized into 10 classes (digits 0 to 9). ‘Fashion-MNIST’ consists of 70,000 grayscale images of fashion items, also 28×28 pixels, divided into 10 classes, including objects

like shirts, trousers, and shoes.

For these experiments, the batch size is $B = 64$ and sub-batch is $N_b = 16$ for all $b \in \mathbb{B}$, the learning rate is 0.0001 for Adam and RMSProp, and $(\rho, \sigma) = (6000, 4000)$ for BADM. As depicted in Fig. 5, BADM exhibits a much faster training speed to achieve the same KID score compared to RMSProp and Adam. For instance, when the KID score reaches -8 dB, the training speed of BADM is at least two times (resp. three times) faster than the others in generating MNIST (resp. Fashion-MNIST) images. The generated images with the same labels are shown in Fig. 6, which exhibit similar qualities but BADM requires much fewer training iterations as illustrated in Fig. 5.

f) Denoising diffusion implicit model (DDIM). We implement another popular generative model, DDIM [32], which can rival GANs in image synthesis quality but incurs higher training costs due to multiple forward passes needed for generating an image. DDIM is a process that gradually transforms an image into noise. By simulating this process, we can create noisy versions of our training images and then train a neural network to denoise them. Once the network is trained, it can perform reverse diffusion during inference, allowing us to generate an image from noise. We use a U-Net with matching input and output dimensions as the architecture of the neural network for denoising. The U-Net network takes two inputs: the noisy images and the variances of their noise components. The variances are necessary because different noise levels necessitate different denoising operations. We transform these noise variances using sinusoidal embeddings, similar to positional encodings used in transformers. This operation enhances the network’s sensitivity to noise levels, which is essential for optimal performance. The training process for DDIM involves uniformly sampling random diffusion times and mixing the training images with Gaussian noise at rates corresponding to the diffusion times. The model is then trained to separate the noisy image into its original image and noise components. Typically, the neural network is trained to predict the unscaled noise component, from which the image component can be derived using the respective signal and noise rates. In this context, the diffusion time is defined as the discrete steps in the forward diffusion process where noise is incrementally added to the data.

The dataset is the Oxford Flowers 102, a diverse collection of approximately 8,000 images of various flower species. The generated images by three algorithms are presented in Fig. 7 and exhibit similar qualities. However, BADM takes fewer training iterations as shown in Fig. 5c.

The dataset is the Oxford Flowers 102, a diverse collection of approximately 8,000 images of various flower species and 20% images are sampled dataset for real-time evaluation. DDIM is trained using this dataset with a batch size of 64. Since DDIM generates colourful images instead of grey-scale images in conditional GANs, this task is more complex, resulting in higher KID values. It can be seen from Fig. 5c that BADM needs the least steps to derive the same KID. The generated images by three algorithms are presented in Fig. 7 and exhibit similar qualities. However, BADM takes fewer training iterations as shown in Fig. 5c.

4.4 Natural Language Processing

This subsection focuses on two NLP tasks. The numerical results demonstrate that BADM is capable of delivering a faster convergence while maintaining the same testing accuracy. Such improvement becomes more evident during pre-training of the language model.

g) Text classification from scratch. Following the example set up in [33], we demonstrate the workflow on the IMDB sentiment classification dataset. The IMDB dataset consists of 25,000 movie reviews with binary sentiment labels indicating positive or negative feedback. We use 20,000 reviews for training and 5,000 reviews for testing. At the beginning of the model, we employ a text vectorization layer for word splitting and indexing. This layer vectorizes the text into integer token IDs, transforming a batch of strings into a dense representation (one sample = 1D array of float values encoding an unordered set of tokens). The 1D CNN consists of 2 convolutional and a fully connected layers, each with 128 kernels. In the experiment, the batch size is $B = 32$, sub-batch is $N_b = 8$, the learning rate is 0.000,2 for Adam and RMSProp, and $(\rho, \sigma) = (1, 000, 4, 000)$ for BADM.

From Fig. 8a³, the training loss for BADM declines dramatically when the iteration number is between 400 and 1,000. The testing accuracy for BADM and RMSProp are both 0.937,5, which is higher than 0.906,2 attained by Adam. Nevertheless, RMSProp displays a slower convergence and its training loss fluctuates significantly.

h) End-to-end masked language modelling (MLM). MLM is a fill-in-the-blank task, where a model uses the context words surrounding a mask token to predict what the masked word is.

Based on the example in [34], the IMDB dataset is used again to evaluate the performance of three algorithms for this task. Similar to the task of text classification, a text vectorization layer is employed. Additionally, we apply a mask function to the input token IDs, randomly masking 15% of all tokens in each sequence. We then construct a BERT-like pre-training model that includes a Multi-Head-Attention layer, which takes token IDs (including masked tokens) as inputs and predicts the correct IDs for these masked tokens. The pre-training model consists of a text vectorization layer, a multi-head attention layer, two fully-connected layers to process the attention output, and one fully-connected layer to predict the masked tokens. After pre-training, we fine-tune a sentiment classification model by creating a classifier by adding a pooling layer and a dense layer on top of the pre-trained BERT features.

For the pre-training experiment, the batch size is $B = 32$, sub-batch is $N_b = 8$, the learning rate is 0.000,1 for Adam and RMSProp, and $(\rho, \sigma) = (8, 000, 2, 000)$ for BADM. For the fine-tuning experiment, all parameters remain the same except for $(\rho, \sigma) = (5, 000, 5, 000)$ for BADM. As shown in Fig. 8b, BADM significantly improves convergence speed during pre-training. The fine-tuning performance is illustrated in Fig. 8c⁴, where all optimizers achieve the same test accuracy of 0.9062, and it can be clearly observed that the training loss of BDAM declines the fastest.

3. Moving average with a window size of 20 for this figure.

4. Moving average with a window size of 10 for this figure.

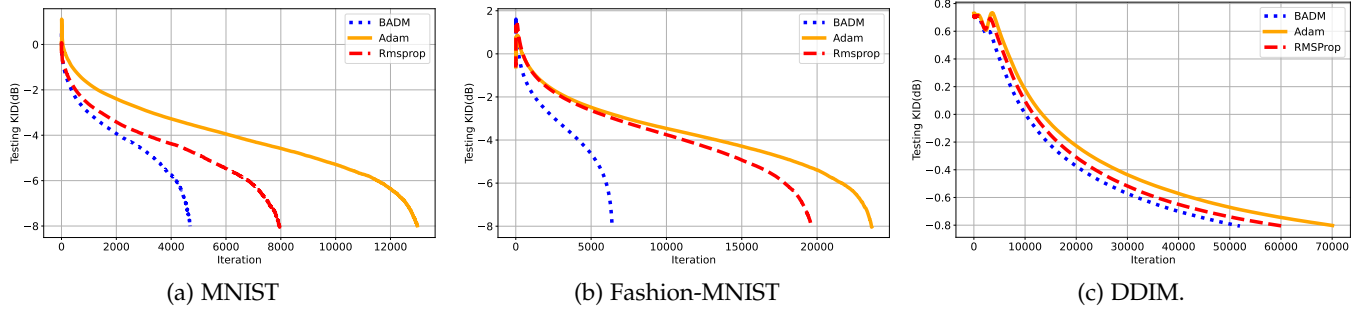


Fig. 5: Testing KID v.s. iterations by conditional GAN and DDIM.

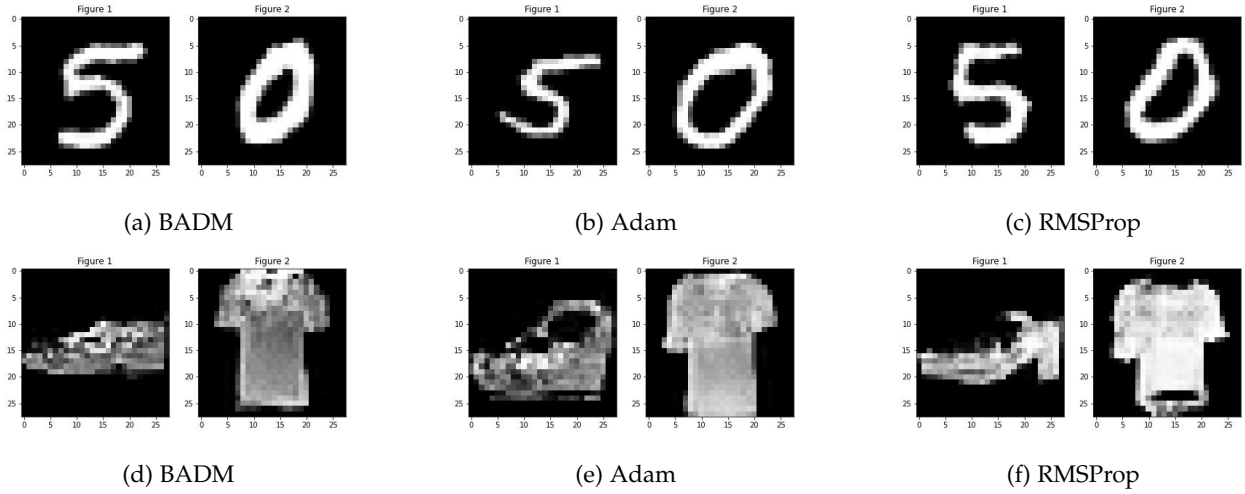


Fig. 6: Generated images using MNIST (Top) and Fashion-MNIST (BOTTOM) datasets.



Fig. 7: Generated images trained using Oxford Flowers dataset.

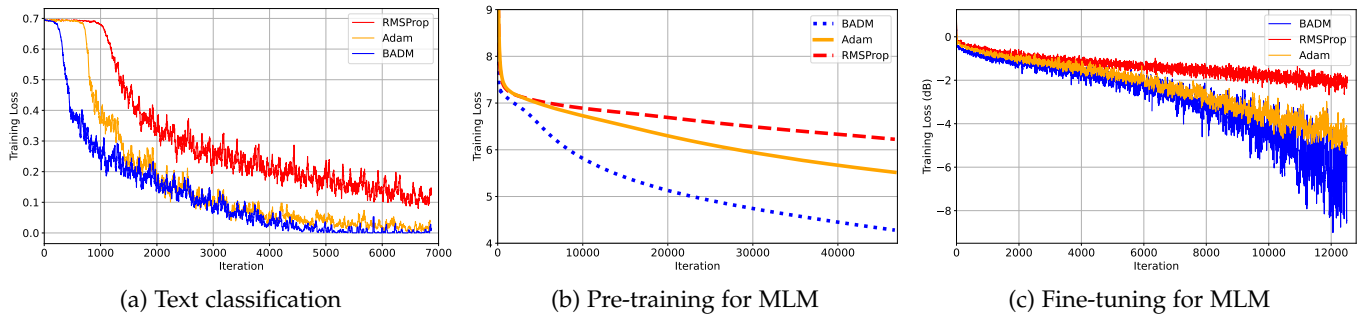


Fig. 8: Training loss v.s. iterations for text classification and MLM.

5 CONCLUSION

Based on the conventional DL training process, we developed an ADMM-type learning algorithm that differs from the conventional ADMM cast to train neural networks. The proposed algorithm can be deemed as a data-driven approach and flexible enough to be applied across a wide range of applications. Extensive numerical experiments have demonstrated its superior performance compared to other state-of-the-art solvers.

REFERENCES

- [1] J. Ho, A. Jain, and P. Abbeel, "Denosing diffusion probabilistic models," *Adv. Neural. Inf. Process. Syst.*, vol. 33, pp. 6840–6851, 2020.
- [2] I. Goodfellow, J. Pouget-Abadie, M. Mirza, B. Xu, D. Warde-Farley, S. Ozair, A. Courville, and Y. Bengio, "Generative adversarial networks," *Commun. ACM*, vol. 63, no. 11, pp. 139–144, 2020.
- [3] O. Wang, J. Gao, and G. Y. Li, "Learn to adapt to new environments from past experience and few pilot blocks," *IEEE Trans. Cogn. Commun. Netw.*, vol. 9, no. 2, pp. 373–385, 2022.
- [4] O. Wang, S. Zhou, and G. Y. Li, "Effective adaptation into new environment with few shots: Applications to ofdm receiver design," in *Proc. 33rd IEEE Int. Wkshp. Mach. Learning Signal Process.* IEEE, 2023, pp. 1–6.
- [5] X. Chen, C. Liang, D. Huang, E. Real, K. Wang, Y. Liu, H. Pham, X. Dong, T. Luong, C.-J. Hsieh *et al.*, "Symbolic discovery of optimization algorithms," in *Proc. 37th Conf. Neural Inform. Process. Syst.*, 2023.
- [6] R. Novak, Y. Bahri, D. A. Abolafia, J. Pennington, and J. Sohl-Dickstein, "Sensitivity and generalization in neural networks: An empirical study," in *Proc. Int. Conf. Learn. Rep.*, 2018.
- [7] N. Qian, "On the momentum term in gradient descent learning algorithms," *Neural Netw.*, vol. 12, no. 1, pp. 145–151, 1999.
- [8] J. Duchi, E. Hazan, and Y. Singer, "Adaptive subgradient methods for online learning and stochastic optimization," *J. Mach. Learn. Res.*, vol. 12, no. 7, 2011.
- [9] T. Tieleman, "Lecture 6.5-rmsprop: Divide the gradient by a running average of its recent magnitude," *COURSERA: Neural Netw. Mach. Learn.*, vol. 4, no. 2, p. 26, 2012.
- [10] D. P. Kingma and J. Ba, "Adam: A method for stochastic optimization," in *Proc. Int. Conf. Learn. Rep.*, 2015.
- [11] T. Dozat, "Incorporating Nesterov Momentum into Adam," in *Proc. Int. Conf. Learn. Rep.*, 2016, pp. 1–4.
- [12] S. Ruder, "An overview of gradient descent optimization algorithms," *arXiv preprint arXiv:1609.04747*, 2016.
- [13] S. Boyd, N. Parikh, E. Chu, B. Peleato, J. Eckstein *et al.*, "Distributed optimization and statistical learning via the alternating direction method of multipliers," *Found. Trends. Mach. Learn.*, vol. 3, no. 1, pp. 1–122, 2011.
- [14] Y. Yang, J. Sun, H. Li, and Z. Xu, "ADMM-csnet: A deep learning approach for image compressive sensing," *IEEE Trans. Pattern Anal. Mach. Intell.*, vol. 42, no. 3, pp. 521–538, 2018.
- [15] S. Zhou and G. Y. Li, "Federated learning via inexact adm," *IEEE Trans. Pattern Anal. Mach. Intell.*, vol. 45, no. 8, pp. 9699–9708, 2023.
- [16] K. Xu, S. Zhou, and G. Y. Li, "Federated reinforcement learning for resource allocation in v2x networks," *arXiv preprint arXiv:2310.09858*, 2023.
- [17] O. Wang, S. Zhou, and G. Y. Li, "New environment adaptation with few shots for ofdm receiver and mmwave beamforming," *arXiv preprint arXiv:2310.12343*, 2023.
- [18] M. Carreira-Perpinan and W. Wang, "Distributed optimization of deeply nested systems," in *Proc. Int. Conf. Artif. Intell. Stat.*, 2014, pp. 10–19.
- [19] A. Gotmare, V. Thomas, J. M. Brea, and M. Jaggi, "Decoupling backpropagation using constrained optimization methods," in *Proc. 35th Int. Conf. Mach. Learn.*, 2018.
- [20] G. Taylor, R. Burmeister, Z. Xu, B. Singh, A. Patel, and T. Goldstein, "Training neural networks without gradients: A scalable ADMM approach," in *Proc. Int. Conf. Mach. Learn.* PMLR, 2016, pp. 2722–2731.
- [21] J. Wang, F. Yu, X. Chen, and L. Zhao, "ADMM for efficient deep learning with global convergence," in *Proc. 25th ACM SIGKDD Int. Conf. Knowl. Discov. Data Min.*, 2019, pp. 111–119.
- [22] J. Wang, H. Li, and L. Zhao, "A convergent ADMM framework for efficient neural network training," *arXiv preprint arXiv:2112.11619*, 2021.
- [23] Z. Ebrahimi, G. Batista, and M. Deghat, "AA-DLADMM: An accelerated ADMM-based framework for training deep neural networks," *arXiv preprint arXiv:2401.03619*, 2024.
- [24] J. Zeng, S.-B. Lin, Y. Yao, and D.-X. Zhou, "On ADMM in deep learning: Convergence and saturation-avoidance," *J. Mach. Learn. Res.*, vol. 22, no. 1, pp. 9024–9090, 2021.
- [25] R. T. Rockafellar and R. J.-B. Wets, *Variational analysis*. Springer Science & Business Media, 2009, vol. 317.
- [26] J. You, Z. Ying, and J. Leskovec, "Design space for graph neural networks," *Adv. Neural Inform. Process. Syst.*, vol. 33, pp. 17 009–17 021, 2020.
- [27] P. Sen, G. Namata, M. Bilgic, L. Getoor, B. Galligher, and T. Eliassi-Rad, "Collective classification in network data," *AI magazine*, vol. 29, no. 3, pp. 93–93, 2008.
- [28] O. Shchur, M. Mumme, A. Bojchevski, and S. Günnemann, "Pitfalls of graph neural network evaluation," in *Proc. Rel. Rep. Learn. Wkshp, NeurIPS 2018*, 2018.
- [29] J. Gilmer, S. S. Schoenholz, P. F. Riley, O. Vinyals, and G. E. Dahl, "Neural message passing for quantum chemistry," in *Proc. Int. Conf. Mach. Learn.* PMLR, 2017, pp. 1263–1272.
- [30] A. Dosovitskiy, L. Beyer, A. Kolesnikov, D. Weissenborn, X. Zhai, T. Unterthiner, M. Dehghani, M. Minderer, G. Heigold, S. Gelly *et al.*, "An image is worth 16x16 words: Transformers for image recognition at scale," in *Proc. Int. Conf. Learn. Rep.*, 2021.
- [31] M. Mirza and S. Osindero, "Conditional generative adversarial nets," *arXiv preprint arXiv:1411.1784*, 2014.
- [32] J. Song, C. Meng, and S. Ermon, "Denosing diffusion implicit models," in *Proc. Int. Conf. Learn. Rep.*, 2021.
- [33] D. S. Sachan, M. Zaheer, and R. Salakhutdinov, "Revisiting lstm networks for semi-supervised text classification via mixed objective function," in *Proc. AAAI Conf. Artif. Intell.*, vol. 33, 2019, pp. 6940–6948.
- [34] J. Salazar, D. Liang, T. Q. Nguyen, and K. Kirchoff, "Masked language model scoring," in *Proc. 58th Ann. Meeting Assoc. Comput. Linguistics*, 2020, pp. 2699–2712.